Journal of Catalysis 369 (2019) 86–94

Contents lists available at ScienceDirect

Journal of Catalysis

journal homepage: www.elsevier.com/locate/jcat

Mechanistic study of methylbenzene dealkylation in methanol-to-olefins catalysis on HSAPO-34

Andrew Hwang, Blake A. Johnson, Aditya Bhan *

Department of Chemical Engineering and Materials Science, University of Minnesota, Minneapolis, MN 55455, USA

ARTICLE INFO

Article history:
Received 14 June 2018
Revised 1 August 2018
Accepted 14 October 2018

Keywords:
Methanol-to-olefins
Methylbenzenes dealkylation
Isotope tracing
Site-specific
Quantitative ^{13}C NMR
HSAPO-34
Methylbenzene flash chromatography

ABSTRACT

Methylbenzenes entrained within the cavities of silicoaluminophosphate zeotype HSAPO-34 react with methanol in H^+-mediated dealkylation to give ethylene and propylene in methanol-to-olefins catalysis. Methylbenzenes dealkylation on solid acids is proposed to occur either via the side-chain mechanism, where an exocyclic C═C undergoes successive methylation prior to C—C cleavage for olefin elimination, or the paring mechanism, where ring contraction to a bicyclohexenyl cation precedes C—C cleavage for olefin elimination. Distinct dealkylation mechanisms prescribe distinct combinations of C atoms—from aromatic methyl, aromatic ring, and methanol/dimethyl ether—to comprise the olefin product. Site-specific isotope tracing that distinguishes between isotope labels in aromatic methyl and aromatic ring positions for each methylbenzene shows that tetramethylbenzene gives ethylene via the side-chain mechanism and penta- and hexamethylbenzene give propylene via the paring mechanism. The ratio of propylene selectivity to ethylene selectivity increases in methanol reactions on HSAPO-34 entrained with a distribution of methylbenzenes deliberately manipulated towards increasing fractions of penta- and hexamethylbenzene, corroborating the conclusion that aromatic precursors and dealkylation mechanisms for ethylene diverge from those for propylene.

1. Introduction

The methanol-to-olefins process is a feedstock agnostic [1,2] route for the production of ethylene and propylene at industrial scale [3,4]. The process utilizes zeotype HSAPO-34 [5–7], a microporous silicoaluminophosphate with CHA topology [8], as a solid acid catalyst. The CHA topology features large ellipsoidal cavities (10×6.7 Å) with narrow apertures (3.8 Å) [8] that preclude ingress and egress of even the simplest branched paraffin, isobutane [6]. These shape-selective properties of HSAPO-34 confer the high light olefins selectivity in methanol-to-olefins processes (C_2–$C_4 \geqslant 90\%$) [3,4]. The methanol-to-olefins reaction on HSAPO-34 proceeds via an indirect, chain carrier mechanism with hybrid inorganic-organic active centers [9]. A silicoaluminophosphate cavity together with the H^+ active site—localized at an oxygen atom bridging silicon and aluminum atoms in the crystalline lattice—comprise the inorganic component, and an unsaturated hydrocarbon entrained within the cavity comprises the organic component [9]. Methylbenzenes constitute the organic component throughout the majority of catalytic turnovers and remain entrained within the cavities during catalysis [9–12]. Methanol engages with an active center in acid-catalyzed methylbenzene dealkylation to give ethylene and propylene [9–13]. The mechanism for methylbenzene dealkylation during methanol-to-olefins catalysis on HSAPO-34 remains unresolved despite industrial practice of the chemistry [3,4] and previous academic investigations with limited experimental [14] but extensive computational [14–22] efforts.

Previous investigations [14–29] consider two proposed mechanisms for aromatic dealkylation on solid acids: the paring [30] and side-chain [31] mechanisms (Scheme 1). Hexamethylbenzene, e.g., undergoes H^+-mediated *gem*-dimethylation in both the paring and side-chain mechanisms. The resulting heptamethylbenzenium ion [32] undergoes, in the paring mechanism, ring contraction to a bicyclohexenyl ion [33] which then undergoes C—C scission to expose a pendant alkyl substituent for olefin elimination. The zeotype conjugate anion (Z^- in Scheme 1) abstracts, in the side-chain mechanism, a proton from a methyl substituent of the heptamethylbenzenium ion to form an exocyclic double bond which serves as the nucleophilic center for successive H^+-mediated methylation preceding olefin elimination. Spectroscopic identification of heptamethylbenzenium and polymethylcyclopentenyl ions entrained within zeotype cavities during methanol-to-olefins catalysis [14,27,34,35] evidence only their formation and does not adjudicate the dealkylation mechanism, and archived

* Corresponding author.
E-mail address: abhan@umn.edu (A. Bhan).

https://doi.org/10.1016/j.jcat.2018.10.022
0021-9517/

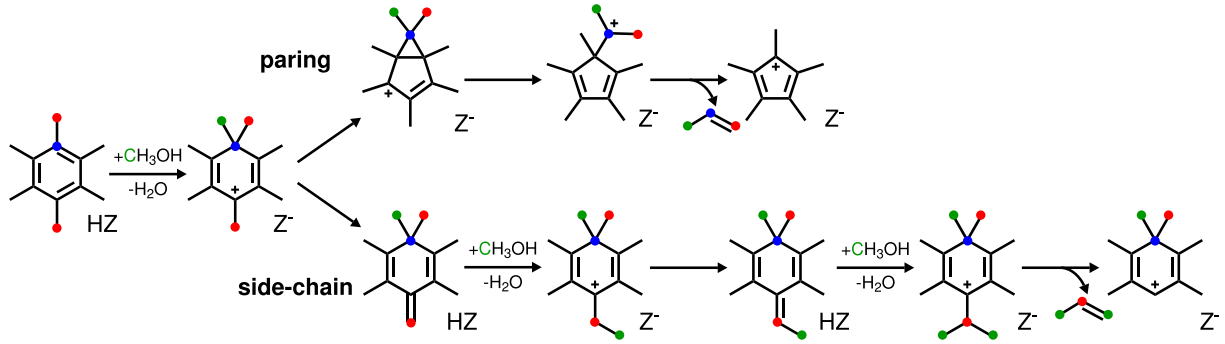

Scheme 1. Dealkylation of hexamethylbenzene for propylene formation via paring and side-chain mechanisms.

elementary step energetics from density functional theory calculations [14–26] lack both the consensus and scope necessary to render unequivocal arbitration of the mechanism.

Isotope tracing studies for methylbenzene dealkylation on medium and large pore zeolites employ methylbenzene co-feeds [28,29,36,37], a stratagem futile for studies with small pore zeotypes, e.g., HSAPO-34, that prevent ingress (and egress) of methylbenzenes. Mechanistic insights afforded by these studies may not extend to small pore zeolites; extrapolation of mechanistic insights across zeotype and zeolite topologies neglects differences in steric and solvation effects, conferred by differences in size and shape of zeotype and zeolite voids, on adsorption and rate constants [16,26,38–40]. Regardless, previous isotope tracing studies on small [14,27], medium [28], and large [29,36,37] pore zeotypes and zeolites lack precision necessary to adjudicate between the side-chain and paring mechanisms (*vide infra*). Unequivocal arbitration of the prevailing dealkylation mechanism requires *site-specific* isotope tracing. The paring mechanism prescribes propylene with one C atom each from the aromatic methyl position, aromatic ring position, and from methanol (●, ●, and ●, respectively, in Scheme 1) while the side-chain mechanism prescribes propylene with one C atom from the aromatic methyl position and two C atoms from methanol. Site-specific isotope tracing that distinguishes between tracers in aromatic methyl (●) and aromatic ring (●) positions provides the precision necessary to arbitrate dealkylation mechanisms and adduce evidence on the mechanistic origins of ethylene and propylene in methanol-to-olefins catalysis.

Here, we employ site-specific isotope tracing to resolve the mechanism for methylbenzenes dealkylation occurring within HSAPO-34 cavities during methanol-to-olefins catalysis. Tetramethylbenzene dealkylation follows the side-chain mechanism to give ethylene, and pentamethylbenzene and hexamethylbenzene dealkylation follow the paring mechanism to give propylene. These mechanistic insights provide opportunity to regulate light olefins selectivity in methanol-to-olefins catalysis by realizing kinetic resolution of ethylene and propylene formation rates afforded by differences in aromatic precursors and dealkylation mechanisms.

2. Results and discussion

A mechanism for methylbenzenes dealkylation—paring, side-chain, or otherwise—prescribes a specific combination of C atoms from methyl substituents of the aromatic (●), ring C atoms of the aromatic (●), and methanol and dimethyl ether (●) to comprise ethylene/propylene. The number of possible combinations of ●, ●, and ● to comprise C_mH_{2m} is $(m+2)!/(2\cdot m!)$. Our protocol for isotope tracing of methylbenzenes dealkylation during methanol-to-olefins catalysis involves an isotope switch reaction and a suite of chromatography and spectrometry techniques to evaluate *total* isotope contents of methanol, dimethyl ether, C_mH_{2m}, and methylbenzenes and *site-specific* isotope contents of methylbenzenes. We assess reaction mechanisms by comparing total isotope contents of C_mH_{2m} ($m = 2$ and 3) with isotope contents of the $(m+2)!/(2\cdot m!)$ combinations (6 and 10 combinations for C_2H_4 and C_3H_6, respectively) calculated from measured isotope contents of ●, ●, and ●. We then consider mechanisms that prescribe the combination with the best match.

We perform a transient isotope switch during methanol-to-olefins catalysis on HSAPO-34 to distribute isotope labels among C_mH_{2m}, methylbenzenes (● and ●), and methanol and dimethyl ether (●). We rapidly quench the reaction some time after the isotope switch and evaluate, instantaneously before the reaction quench, the total isotope contents of species appearing in the fluid phase (i.e., C_mH_{2m} and ●) using typical online gas chromatography/mass spectrometry (GC/MS) protocols combined with matrix deconvolution methods [41]. We then dissolve the silicoaluminophosphate in aqueous hydrochloric acid to liberate the methylbenzenes [42,43] and use GC/MS, liquid chromatography, and quantitative ^{13}C NMR spectroscopy to evaluate total and site-specific isotope contents of the once entrained methylbenzenes (● and ●). (See Methods section for complete details on experimental methodology.) The exquisite positional resolution afforded by ^{13}C NMR spectroscopy enables discrimination between ^{13}C labels in aromatic ring versus aromatic methyl positions. Such discrimination is impossible via deconvolution of electron ionization mass spectra because of low sensitivity—negligible fragmentation to CH_3 and C_6H_x ions—and corruptions from intra- and interfragment isotope scrambling upon high-energy (70 eV) electron impact.

The site-specific ^{13}C contents in aromatic methyl positions and aromatic ring positions for a methyl-substituted benzene with n methyl substituents, i.e., $(CH_3)_nC_6H_{6-n}$, are

$$\frac{^{13}C_{n,\text{methyl}}}{^{12}C_{n,\text{methyl}} + {}^{13}C_{n,\text{methyl}}} \tag{1}$$

and

$$\frac{^{13}C_{n,\text{ring}}}{^{12}C_{n,\text{ring}} + {}^{13}C_{n,\text{ring}}}, \tag{2}$$

respectively, where $^xC_{n,y}$ is the number of C atoms in $(CH_3)_nC_6H_{6-n}$ with mass number x in position y. Quantification of site-specific ^{13}C contents (Eqs. (1) and (2)) requires determining the set $\{^xC_{n,y}\}$ ($x = 12$ or 13, $y =$ methyl or ring). The following set of four linearly independent equations gives a unique solution for $\{^xC_{n,y}\}$:

$$^{12}C_{n,\text{methyl}} + {}^{13}C_{n,\text{methyl}} + {}^{12}C_{n,\text{ring}} + {}^{13}C_{n,\text{ring}} = n + 6 \quad (3)$$

$$\frac{^{12}C_{n,\text{methyl}} + {}^{13}C_{n,\text{methyl}}}{^{12}C_{n,\text{ring}} + {}^{13}C_{n,\text{ring}}} = \frac{n}{6} \quad (4)$$

$$\frac{^{13}C_{n,\text{methyl}} + {}^{13}C_{n,\text{ring}}}{^{12}C_{n,\text{methyl}} + {}^{13}C_{n,\text{methyl}} + {}^{12}C_{n,\text{ring}} + {}^{13}C_{n,\text{ring}}} = \mu_n \quad (5)$$

$$\frac{^{13}C_{n,\text{ring}}}{^{13}C_{n,\text{methyl}}} = \nu_n. \quad (6)$$

Eqs. (3) and (4) arise from speciation of a methyl-substituted benzene; $(CH_3)_nC_6H_{6-n}$ has $n+6$ total C atoms and $n/6$ methyl C atoms to ring C atoms. Eq. (5) expresses the total ^{13}C content of $(CH_3)_nC_6H_{6-n}$ (μ_n). Matrix deconvolution of electron ionization mass spectra of methylbenzenes, acquired in GC/MS analysis of the mixture of liberated methylbenzenes, gives isotopologue distributions to calculate μ_n values. Eq. (6) expresses the relative ^{13}C enrichment in aromatic ring versus aromatic methyl positions (ν_n). Integration of quantitative ^{13}C NMR spectra, acquired for each methylbenzene after separation of the mixture of methylbenzenes using reverse-phase flash chromatography, gives ν_n values.

The measurement of ν_n during methanol-to-olefins catalysis distinguishes the *site-specific* isotope tracing study reported here from previous isotope tracing studies of methylbenzenes dealkylation [14,27–29,36,37]. Mathematically, this measurement supplies the fourth linearly independent equation (Eq. (6)) necessary to give a unique solution for the set of four independent variables $\{^xC_{n,y}\}$; without this, there exist infinite possible solutions to the undetermined system of equations [44]. A unique solution confers precision to *site-specific* isotope tracing and avoids ambiguity inherent to undetermined systems. Previous attempts to circumvent this ambiguity rely on presumption that isotope labels, when conveyed by methanol/dimethyl ether, preferentially populate aromatic methyl positions in methylbenzenes [14,27,28,37] or that the distribution of isotope labels, among aromatic methyl and aromatic ring carbons, in a co-fed methylbenzene remains undisturbed after many dealkylation turnovers [29,36]. We instead deploy liquid chromatography and quantitative ^{13}C NMR spectroscopy to measure ν_n values and calculate *site-specific* isotope contents in aromatic methyl and aromatic ring positions (Eqs. (1) and (2), respectively) for each methylbenzene during methanol-to-olefins catalysis on HSAPO-34.

Table 1 lists the reaction conditions (temperature, influent methanol concentration, and space velocity) for three independent isotope switching ($^{13}CH_3OH$ to $^{12}CH_3OH$) reactions performed on fixed beds of HSAPO-34. Table 1 also lists the turnover number [45] at the isotope switch, the thermal reaction quench, and complete deactivation. Turnover number tracks reaction progress in terms of the moles of methanol converted to hydrocarbon products per mole of H^+ [45]. The turnover number at complete deactivation is an intensive assessment of catalyst lifetime [45–48]. The distribution of products appearing in the fixed-bed effluent and the distribution of organic species entrained within HSAPO-34 during methanol-to-olefins catalysis are both sensitive to turnover number [45]. (See Supporting Information for definition of turnover number and profiles of conversion and turnover number versus time-on-stream for reactions **1**, **2**, and **3** (Table 1).) We, in the three independent isotope switching reactions, varied the turnover number at the thermal reaction quench with intent to vary the sampled distribution of methylbenzenes entrained within the silicoaluminophosphate cavities, and we varied the difference between the turnover number at the isotope switch and that at the thermal reaction quench with intent to vary the extent of ^{12}C incorporation in effluent olefins and entrained methylbenzenes. We avoided switching and quenching at early turnovers ($\leqslant 50\ \text{mol}_C\ \text{mol}_{H^+}^{-1}$) to avoid contributions to isotope contents of C_mH_{2m} from olefins β-scission [45].

Table 2 lists the ^{13}C contents of C_2H_4, C_3H_6, ●, ●, and ● for reactions **1**, **2**, and **3** (Table 1). The ^{13}C content ascribed to ● is the arithmetic mean of the ^{13}C contents of methanol and dimethyl ether, either can convey CH_3^+ in H^+-mediated methylation steps within elementary step sequences for methylbenzenes dealkylation. The degree of ^{12}C incorporation in methylbenzenes upon switching from $^{13}CH_3OH$ to $^{12}CH_3OH$ increases with increasing number of methyl substituents for all reactions **1**, **2**, and **3**, i.e., the total ^{13}C content of $(CH_3)_nC_6H_{6-n}$ (μ_n) decreases with n. This trend is consistent with previous reports [15,19,21,36,49] suggesting that rates of dealkylation increase with increasing number of methyl substituents—hexamethylbenzene incorporates more ^{12}C than toluene upon switching from $^{13}CH_3OH$ to $^{12}CH_3OH$ because active centers with hexamethylbenzene as the organic component turn over faster than those with toluene. Thus, we consider only tetra-, penta-, and hexamethylbenzene as precursors for ethylene and propylene in the following analysis.

Table 3 lists, for each $(CH_3)_nC_6H_{6-n}$ ($n = 4,\ 5,$ and 6), the calculated ^{13}C contents for the six possible combinations of ●, ●, and ● to comprise C_2H_4 in reactions **1**, **2**, and **3** (Table 1). The ^{13}C content of the combination ● + ● for tetramethylbenzene in reaction **1** (27%, Table 3), e.g., is calculated as one-half the sum of the ^{13}C content of the aromatic ring position (●) of tetramethylbenzene in reaction **1** (52%, Table 2) and the ^{13}C content of methanol/dimethyl ether (●) in reaction **1** (1.7%, Table 2). Table 3 also lists the absolute relative error between the measured ^{13}C content of C_2H_4 and the calculated ^{13}C content of each combination. The absolute relative error for the combination ● + ● for tetramethylbenzene in reaction **1** (55%, Table 3), e.g., is the absolute difference between the measured ^{13}C content of C_2H_4 in reaction **1** (17%, Table 2) and the calculated ^{13}C content of ● + ● from tetramethylbenzene in reaction **1** (27%, Table 3) normalized by the measured ^{13}C content of C_2H_4 in reaction **1** (17%, Table 2). The entries of Table 3 shaded in gray denote the combination resulting in the smallest absolute relative error when averaged across reactions **1**, **2**, and **3** (Table 1).

Table 1
Reaction Conditions for Transient $^{13}CH_3OH$ to $^{12}CH_3OH$ Switch during Methanol-to-Olefins Catalysis on HSAPO-34

	T / K	$P_{MeOH,0}$ / kPa	Space velocity / $\left(\text{MeOH}\ (H^+ \cdot \text{ks})^{-1}\right)$	Turnover Number / $\left(\text{mol}_C\ \text{mol}_{H^+}^{-1}\right)$		
				Switch	Quench	Complete deactivation
1	598	12	65	54	62	146
2	598	12	150	61	64	96
3	598	12	47	134	135	152

Space velocity = (Influent molar flow rate of methanol)/(Moles of H^+ in catalyst bed).
Turnover number = $\int dt$ [(Space velocity) · (Fractional conversion of methanol to hydrocarbons)].

Table 2
^{13}C Contents of Ethylene, Propylene, Methanol, Dimethyl Ether, and Methylbenzenes Measured in Transient Isotope Switching Reactions **1**, **2**, and **3** (Table 1).

	^{13}C Content/%								
	1			**2**			**3**		
C_2H_4	17			39			39		
C_3H_6	20			38			39		
CH_3OH	0			1.9			18		
CH_3OCH_3	3.5			3.8			3.6		
●	1.7			2.9			11		
	●	●	μ_n	●	●	μ_n	●	●	μ_n
$(CH_3)_1C_6H_5$	nm	nm	84	nm	nm	98	94	99	98
$(CH_3)_2C_6H_4$	nm	nm	75	82	97	93	100	96	97
$(CH_3)_3C_6H_3$	nm	nm	70	74	90	85	81	96	91
$(CH_3)_4C_6H_2$	25	52	42	64	58	60	64	86	77
$(CH_3)_5C_6H_1$	17	50	35	33	66	51	23	83	56
$(CH_3)_6C_6H_0$	13	42	27	34	69	51	20	84	52

nm = not measured.
1, **2**, **3** correspond to reaction conditions listed in Table 1.
● = ^{13}C content of aromatic methyl position.
● = ^{13}C content of aromatic ring position.
● = Average ^{13}C content of CH_3OH and CH_3OCH_3.
μ_n = Total ^{13}C content of $(CH_3)_nC_6H_{6-n}$ (see Eq. (5)).

Table 3
^{13}C Contents of the Six Possible Combinations of C Atoms from ●, ●, and ● to Comprise Ethylene.

	^{13}C Content / % (Absolute Relative Error / %)											
	1			**2**			**3**			**Average**		
$(CH_3)_nC_6H_{6-n}$	4	5	6	4	5	6	4	5	6	4	5	6
● + ●	25 (46)	17 (2.7)	13 (26)	64 (62)	33 (17)	34 (14)	64 (61)	23 (43)	20 (48)	— (56)	— (21)	— (29)
● + ●	39 (120)	33 (91)	27 (56)	61 (55)	49 (25)	51 (30)	75 (90)	53 (34)	52 (33)	— (88)	— (50)	— (40)
● + ●	14 (22)	9.3 (46)	7.3 (58)	33 (16)	18 (55)	18 (53)	37 (5.4)	17 (57)	16 (60)	— (14)	— (53)	— (57)
● + ●	52 (200)	50 (190)	42 (140)	58 (48)	66 (67)	69 (75)	86 (120)	83 (110)	84 (110)	— (120)	— (120)	— (110)
● + ●	27 (55)	26 (48)	22 (24)	31 (22)	34 (13)	36 (9.0)	49 (23)	47 (20)	48 (21)	— (33)	— (27)	— (18)
● + ●	1.7 (90)	1.7 (90)	1.7 (90)	2.9 (93)	2.9 (93)	2.9 (93)	11 (72)	11 (72)	11 (72)	— (85)	— (85)	— (85)

1, **2**, **3** correspond to reaction conditions listed in Table 1.
Entries in column labeled **Average** are the arithmetic mean of absolute relative errors of entries in **1**, **2**, and **3**.
● = Aromatic methyl.
● = Aromatic ring.
● = CH_3OH and CH_3OCH_3.
See Table 2 for ^{13}C contents of ●, ●, ●, and ethylene.
Absolute Relative Error = $\frac{|(^{13}C \text{ content of combination}) - (^{13}C \text{ content of ethylene})|}{(^{13}C \text{ content of ethylene})}$.

The calculated ^{13}C contents of the combination ● + ● from $(CH_3)_4C_6H_2$ give, when averaged across reactions **1**, **2**, and **3**, the best match to the measured ^{13}C contents of C_2H_4 (14% absolute relative error, Table 3). The side-chain mechanism for dealkylation of tetramethylbenzene (Scheme 2) prescribes exactly ● + ● for ethylene. The steps drawn in Scheme 2 adhere to, in general, the first proposal for the side-chain mechanism [31], and the intermediates depicted conform to stationary points along reaction trajectories for side-chain dealkylation of methylbenzenes identified with density functional theory calculations [15,17,21,22]. 1,2,4,5-tetramethylbenzene, e.g., reacts with methanol/dimethyl ether at a proton to give a benzenium ion with a *gem*-dimethyl substituent. This cation undergoes deprotonation to form a substituted cyclohexadiene with a methylene moiety *para* to the *gem*-dimethyl. H^+-mediated methylation at the exocyclic methylene gives an ethyl substituent comprised of a C atom originating from the aromatic methyl position (●) and a C atom from methanol/dimethyl ether (●). Subsequent C—C cleavage gives ethylene; archived reaction trajectories from computational efforts include hydride shifts [17], methyl shifts [21,22], or spiro formation [17,26] prior to C—C

cleavage while others suggest direct α-scission without intervening steps [15]. The provenance of C atoms comprising ethylene, ● + ●, is identical to the ethyl substitutent regardless of steps intervening methylene methylation and the ultimate C—C cleavage.

The paring mechanism, when initiated by protonation of a methylbenzene [30] instead of *gem*-dimethylation (Scheme 1), prescribes ethylene with the combination ● + ●. This combination results in ⩾ 40% absolute relative error compared to 14% for the combination prescribed by the side-chain mechanism for tetramethylbenzene dealkylation. The paring mechanism for dealkylation of hexamethylbenzene, when initiated by *gem*-dimethylation as drawn in Scheme 1, cannot give ethylene. The paring mechanism for dealkylation of pentamethylbenzene and lower homologues, when initiated by *gem*-dimethylation, can give ethylene if a methyl-shift precedes C—C scission at the cyclopropyl moiety. This mechanism prescribes ethylene with the combination 0.5 ● + ● + 0.5 ● since either methyl of the *gem*-dimethyl substitutent (● or ●) can shift. This combination gives larger absolute relative error (⩾ 28%) compared to the combination prescribed by the side-chain mechanism for tetramethylbenzene dealkylation.

Table 4 is analogous to Table 3 but for C_3H_6 instead of C_2H_4. The calculated ^{13}C contents of the combination ● + ● + ● from $(CH_3)_5C_6H_1$ and $(CH_3)_6C_6H_0$ give the best match to the measured ^{13}C contents of C_3H_6 (9.0% and 4.7% absolute relative error, respectively; Table 4). The paring mechanism for dealkylation of penta- and hexamethylbenzene (Scheme 3) prescribes exactly ● + ● + ● for propylene. Again, the steps drawn in Scheme 3 adhere to, in general, the first proposal for the paring mechanism [30], and the intermediates depicted conform to stationary points along reaction trajectories for dealkylation of methylbenzenes via the paring mechanism identified with density functional theory calculations [14,19,25]. Hexamethylbenzene, e.g., reacts with methanol/dimethyl ether at a proton to give a heptamethylbenzenium ion which undergoes ring contraction to form a methyl-substituted bicyclohexenyl cation. Ring opening at the cyclopropyl moiety exposes a pendant propyl substituent on a methyl-substituted cyclopentadienyl cation which undergoes C—C scission to give propylene. The side-chain mechanism prescribes propylene with the combination ● + ● + ● which gives ⩾ 39% absolute relative error compared to the ⩽ 9.0% absolute relative error for the paring mechanism.

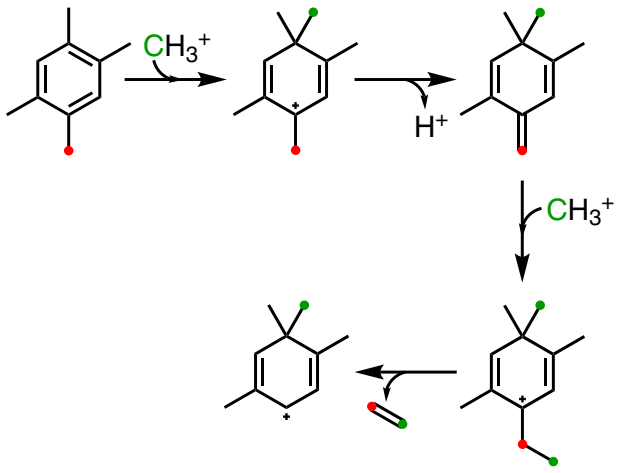

Scheme 2. Side-chain mechanism for dealkylation of tetramethylbenzene for ethylene formation.

The results of this isotope tracing study suggest that methanol-to-olefins catalysis on HSAPO-34 distinguishes aromatic precursors and dealkylation mechanisms for ethylene formation from those for propylene formation. Tetramethylbenzene undergoes dealkylation via the side-chain mechanism to give ethylene, and pentamethylbenzene and hexamethylbenzene undergo dealkylation via the paring mechanism to give propylene. Implicit in our approach thus far is a presumption of one-to-one correspondence between a combination of C atoms that comprise ethylene/propylene and a mechanism for the dealkylation of tetra-, penta- and/or hexamethylbenzene. It is possible that the isotope content of C_mH_{2m} reflects instead a conflation of many combinations prescribed from many pathways. In general, each $(CH_3)_nC_6H_{6-n}$ can undergo dealkylation via many distinct mechanisms (p) that together prescribe ethylene and propylene with a rate-weighted average of isotope contents prescribed by each distinct dealkylation pathway, i.e.,

$$(\text{Isotope content of } C_mH_{2m}) = \frac{\sum_n \sum_p (\text{Isotope content prescribed to } C_mH_{2m} \text{ by mechanism } p \text{ for dealkylation of } (CH_3)_nC_6H_{6-n}) \cdot (\text{Rate of dealkylation of } (CH_3)_nC_6H_{6-n} \text{ to } C_mH_{2m} \text{ via mechanism } p)}{\sum_n \sum_p (\text{Rate of dealkylation of } (CH_3)_nC_6H_{6-n} \text{ to } C_mH_{2m} \text{ via mechanism } p)}. \quad (7)$$

An isotope tracing study alone affords little or no mechanistic insight when multiple dealkylation pathways operate, with similar kinetic feasibility, to give ethylene and propylene. The excellent agreements between measured isotope contents of ethylene and the isotope contents of combinations prescribed by the side-chain mechanism for tetramethylbenzene dealkylation to ethylene and the excellent agreements between isotope contents of propylene and the isotope contents prescribed by the paring mechanism for penta- and hexamethylbenzene dealkylation to propylene suggest, however, fidelity to the presumed one-to-one correspondence. Instead of the most general case (Eq. (7)), the results of the isotope tracing study imply a special case where for $m = 2, n = 4$ and $p =$ side-chain and for $m = 3, n = 5$ and 6 and $p =$ paring. We pursued additional evidence to corroborate this conclusion by examining selectivity transients during methanol-to-olefins catalysis on HSAPO-34 upon deliberate manipulation of the distribution of entrained methylbenzenes.

Scheme 4 shows the distribution of methylbenzenes entrained within HSAPO-34 after 1.8 ks of reaction of 12 kPa MeOH at 598 K and 100 MeOH $(H^+ \cdot ks)^{-1}$. The molar ratio of pentamethylbenzene and hexamethylbenzene to tetramethylbenzene entrained within HSAPO-34 for this described reaction is 0.6 (Scheme 4, *(5 + 6)/4 = 0.6*). The results of the isotopic tracing study suggest tetramethylbenzene as the aromatic precursor for ethylene and pentamethylbenzene and hexamethylbenzene as the aromatic precursors for ethylene. An increase in the ratio of propylene selectivity to ethylene selectivity with increasing molar ratio of entrained pentamethylbenzene and hexamethylbenzene to entrained tetramethylbenzene would corroborate this interpretation of the isotopic tracing results. We envisioned that subsequent reaction of methanol at lower temperatures would effect homologation of entrained methylbenzenes to shift the distribution towards hexamethylbenzene (Scheme 4). As anticipated, the fraction of hexamethylbenzene increases from 2.1% (mol basis) to 12% and the fraction of tetramethylbenzene decreases from 37% to 30% upon subsequent reaction of 12 kPa MeOH at 423 K and

Table 4
^{13}C Contents of the Ten Possible Combinations of C Atoms from ●, ●, and ● to Comprise Propylene.

	^{13}C Content / % (Absolute Relative Error / %)											
	1			**2**			**3**			**Average**		
$(CH_3)_nC_6H_{6-n}$	4	5	6	4	5	6	4	5	6	4	5	6
●+●+●	25 (27)	17 (15)	13 (36)	64 (67)	33 (15)	34 (11)	64 (65)	23 (42)	20 (47)	— (53)	— (24)	— (31)
●+●+●	34 (72)	28 (40)	22 (12)	62 (62)	44 (14)	45 (19)	71 (84)	43 (11)	42 (8.0)	— (73)	— (22)	— (13)
●+●+●	18 (12)	12 (40)	9.1 (54)	43 (14)	23 (41)	24 (38)	46 (19)	19 (52)	17 (55)	— (15)	— (44)	— (49)
●+●+●	43 (120)	39 (95)	32 (61)	60 (58)	55 (43)	57 (50)	79 (104)	63 (63)	63 (63)	— (94)	— (67)	— (58)
●+●+●	26 (33)	23 (14)	19 (6.1)	42 (9.1)	34 (12)	35 (7.9)	54 (39)	39 (0.85)	39 (0.18)	— (27)	— (9.0)	— (4.7)
●+●+●	9.6 (52)	6.8 (66)	5.4 (73)	23 (39)	13 (67)	13 (65)	28 (26)	15 (62)	14 (64)	— (39)	— (65)	— (67)
●+●+●	52 (160)	50 (150)	42 (110)	58 (53)	66 (73)	69 (80)	86 (120)	83 (120)	84 (120)	— (111)	— (114)	— (103)
●+●+●	35 (78)	34 (69)	28 (42)	40 (4.4)	45 (18)	47 (23)	61 (59)	59 (53)	60 (55)	— (47)	— (47)	— (40)
●+●+●	19 (6.8)	18 (11)	15 (25)	21 (44)	24 (37)	25 (35)	36 (6.6)	35 (9.2)	35 (8.4)	— (19)	— (19)	— (23)
●+●+●	1.7 (91)	1.7 (91)	1.7 (91)	2.9 (92)	2.9 (92)	2.9 (92)	11 (72)	11 (72)	11 (72)	— (85)	— (85)	— (85)

1, **2**, **3** correspond to reaction conditions listed in Table 1.
Entries in column labeled **Average** are the arithmetic mean of absolute relative errors of entries in **1**, **2**, and **3**.
● = Aromatic methyl.
● = Aromatic ring.
● = CH_3OH and CH_3OCH_3.
See Table 2 for ^{13}C contents of ●, ●, ●, and propylene.
Absolute Relative Error = $\frac{|(^{13}\text{C content of combination})-(^{13}\text{C content of propylene})|}{(^{13}\text{C content of propylene})}$.

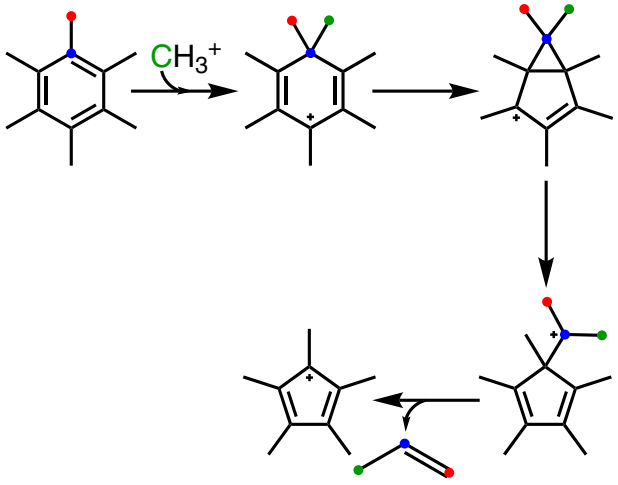

Scheme 3. Paring mechanism for dealkylation of hexamethylbenzene for propylene formation.

100 MeOH $(H^+ \cdot ks)^{-1}$ for 72 ks. The molar ratio of pentamethylbenzene and hexamethylbenzene to tetramethylbenzene, upon this subsequent methanol reaction at 423 K, increases from 0.6 to 1.0 (Scheme 4). The distribution shifts further towards hexamethylbenzene when the subsequent methanol reaction is performed instead at 448 K, increasing the molar ratio of pentamethylbenzene and hexamethylbenzene to tetramethylbenzene to 1.4. We, having established a protocol for shifting the distribution of entrained methylbenzenes towards those expected as precursors for propylene, performed reaction of 12 kPa MeOH at 598 K and 100 MeOH $(H^+ \cdot ks)^{-1}$ on HSAPO-34 entrained with the unmanipulated (*(5 + 6)/4 = 0.6*; reaction **4** in Scheme 4) and manipulated (*(5 + 6)/4 = 1.0* and *(5 + 6)/4 = 1.4* reactions **5** and **6**, respectively, in Scheme 4) distributions of methylbenzenes.

Fig. 1 shows the ratio of propylene selectivity to ethylene selectivity versus turnover number for reactions **4**, **5**, and **6** (Scheme 4). The ratio remains nearly constant at 1.8 throughout one turnover for the reaction on HSAPO-34 entrained with the unmanipulated

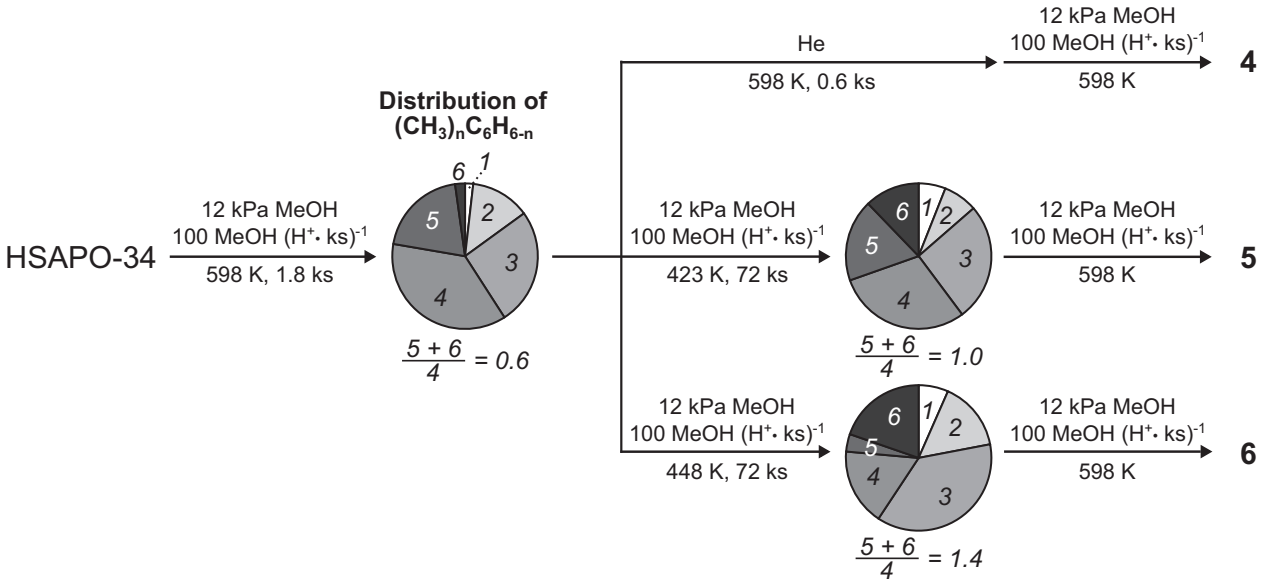

Scheme 4. Manipulation of the distribution of entrained methylbenzenes via low temperature homologation.

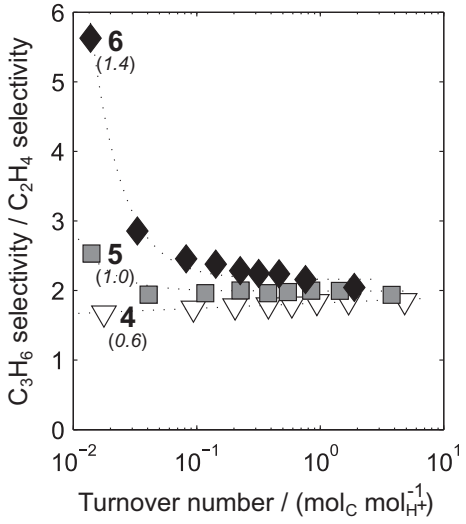

Fig. 1. Ratio of propylene selectivity (C basis) to ethylene selectivity (C basis) versus turnover number for reactions **4** (▽), **5** (■), and **6** (◆) (Scheme 4). The molar ratio of pentamethylbenzene and hexamethylbenzene to tetramethylbenzene entrained within the HSAPO-34 cavities, i.e., (*(5 + 6)/4* in Scheme 4), is 0.6, 1.0, and 1.4 for reactions **4**, **5**, and **6**, respectively. Dotted lines are guides for the eye.

disitribution of methylbenzenes (reaction **4** in Scheme 4). The initial propylene-to-ethylene selectivity increases to 2.5 in reaction **5** (Scheme 4) before decreasing asymptotically towards 1.8, and the initial propylene-to-ethylene selectivity increases further to 5.6 in reaction **6** (Scheme 4). (The manipulated distributions of entrained methylbenzenes trend, apparently, towards the unmanipulated distribution with turnover as reflected by the aymptotically decreasing propylene-to-ethylene selectivity.) These trends corroborate a conclusion of the isotopic tracing study that pentamethylbenzene and hexamethylbenzene are the aromatic precursors for propylene and tetramethylbenzene is the aromatic precursor for ethylene.

The site-specificity of this isotope tracing study renders the precision necessary for experimental arbitration of the mechanism for methylbenzene dealkylation. The results provide mechanistic rationale for the previously reported observation of increased propylene selectivity and decreased ethylene selectivity with increasing average number of methyl substituents of entrained methylbenzenes [49], and they also complement spectroscopic studies [14,35] that identify heptamethylbenzenium and methylcyclopentenyl ions as intermediates in methylbenzenes dealkylation on HSAPO-34.

Computational studies that attempt to arbitrate methylbenzenes dealkylation mechanisms on HSAPO-34 [14,19] conclude that the side-chain mechanism is more energetically favorable than the paring mechanism for propylene formation, in apparent conflict with the results of our experimental study. We cannot, at this time, provide a decisive explanation for the discrepancy between these calculations [14,19] and our experimental results. We note that these computational studies [14,19] arbitrate mechanisms by comparing calculated energy barriers at 0 K while reaction trajectories in our experimental setting traverse Gibbs free energy surfaces at 598 K. A computational study that reports calculated Gibbs free energy barriers (and calculated rate constants) for methylbenzenes dealkylation on HSAPO-34 [21] lacks the scope necessary to arbitrate the mechanism as the report includes only two reaction trajectories: one for ethylene formation and one for propylene formation in hexamethylbenzene dealkylation via the side-chain mechanism.

3. Conclusions

The mechanism for methylbenzenes dealkylation during methanol-to-olefins catalysis on HSAPO-34 depends on the identity of the aromatic precursor. Site-specific isotope tracing that distinguishes isotope labels in aromatic ring versus aromatic methyl positions shows that the side-chain mechanism prevails for tetramethylbenzene dealkylation to give ethylene (Scheme 2) and the paring mechanism prevails for penta- and hexamethylbenzene to give propylene (Scheme 3). The ratio of propylene selectivity to ethylene selectivity increases with increasing extent of homologation within the pool of entrained methylbenzenes consistent with the conclusion that distinct methylbenzenes undergo dealkylation via distinct mechanisms to give distinct olefin products.

4. Methods

The preparation and characterization of the SAPO-34 sample was previously reported [50]. The powder X-ray diffractogram and micropore volume are consistent with the CHA topology; the crystallites are cubic in morphology with size of ca. 1 μm; the (Al + P)/Si ratio is 12; and the Brønsted acid site density is $0.85 \cdot 10^{-3}$ mol H^+ g^{-1}. The SAPO-34 sample was stored with the cationic moiety of the organic structure directing agent ($(C_2H_5)_4N^+$) intact, i.e., as the charge balancing counterion, to avoid modifications to the coordinative environment of Si heteroatoms [51] and only de-templated, and converted to H^+ form, via thermal oxidative treatment immediately prior to catalytic testing (*vide infra*).

Methanol-to-olefins reactions were performed on fixed-beds comprised of SAPO-34 aggregates (180–250 μm) mixed with quartz granules (180–250 μm; washed with 2 M HNO_3(aq), rinsed with deionized water, and treated in flowing dry air at 1273 K for 12 h; 5:1 g_{SiO_2}:$g_{SAPO-34}$). Catalyst beds were supported on a porous quartz disc within a "U"-shaped tubular quartz reactor (1.0 cm i.d.). The reactor was placed within a resistively heated furnace (National Element FA120); the reaction temperature was regulated by an electronic controller (Watlow 96) and measured by a K-type thermocouple fixed within a dimple at the reactor wall located near the axial center and penetrating through to the radial center of the catalyst bed. Catalyst beds were treated in flowing air (3.33 cm^3 s^{-1} g^{-1}; Matheson, Ultra Zero Certified) at 873 K for 8 h (0.0167 K s^{-1}) prior to methanol-to-olefins reaction. Liquid methanol ($^{12}CH_3OH$, Fluka ⩾ 99.9%; $^{13}CH_3OH$, Cambridge Isotope Laboratories, ⩾99 atom% ^{13}C) was delivered by a syringe pump (Cole-Parmer 780100C) and vaporized into heated gas transfer lines (ca. 393 K) with flowing He (Minneapolis Oxygen, ⩾99.997%); He flow rates were metered using thermal mass flow controllers (Brooks SLA5850). Concentrations of species in reactor influent and effluent mixtures were quantified using a gas chromatograph (Agilent 7890) equipped with a polystyrene-divinylbenzene column (HP-PLOT Q, 30 m × 0.530 mm × 40 μm) connected in series to a molecular-sieve coated column (CP-Molsieve 5 Å, 25 m × 0.530 mm × 50 μm) with an intervening two-position, six-port valve (VICI Valco); the train of columns was connected in series to first, a thermal conductivity detector; then, an oxidation-methanation reactor (Polyarc®, Activated Research Company); and finally, a flame ionization detector. Mass fragmentation patterns were collected using gas chromatography-mass spectrometry (Agilent 5975C; HP-PLOT Q, 30 m × 0.32 mm × 20 μm) and deconvoluted using matrix methods [41] to determine isotoplogue distributions and calculate ^{13}C contents. Thermal quenching of reactions (−10 K s^{-1}) was performed by rapidly displacing the resistively heated furnace with desk fans.

The contents of the catalyst bed, upon thermal quench, were placed in a glass vial and suspended in 4 M HCl(aq) (37 wt% HCl; Sigma-Aldrich, ACS Reagent) for 0.5 h via magnetic stirring with a PTFE-coated stir bar to effect SAPO-34 dissolution [42,43]; the resulting suspension was neutralized by addition of NaOH (Sigma-Aldrich, ⩾99.99%) and filtered using a syringe filter (Millex-FH; 0.45 μm, PTFE), and methanol (Fisher-Scientific, HPLC grade) was added to solubilize methylbenzenes. The mixture of methylbenzenes in methanol-water was separated using reverse-phase flash chromatography (Sorbtech C_{18}; 15–19% C, 100 Å, 20–45 μm) with gradient elution using solutions of methanol (Fisher-Scientific, HPLC grade) and water (Fisher-Scientific, HPLC grade) as the mobile phase. Separation was verified using the previously described gas chromatography protocols. Samples for NMR were prepared by concentrating methylbenzenes, from the column eluent, by liquid-liquid extraction into cyclohexane-d_{12} (Cambridge Isotope Laboratories, ⩾99.6 atom% D). ^{13}C NMR spectra were collected using a Bruker Avance NEO spectrometer equipped with a 5 mm TCI cryoprobe and operating at 14.1 T and 150.031 MHz ^{13}C NMR frequency. Quantitative ^{13}C NMR spectra were obtained by adding chromium acetylacetonate (Sigma-Aldrich, 97%) and using an inverse-gated decoupling pulse sequence [52,53]; ^{13}C NMR spectra were acquired with a 14 μs pulse delay, a 2 s delay time, and 10^4–10^5 scans. The efficacy of the quantification was verified by integration of a ^{13}C NMR spectrum acquired for a standard sample of 1000 ppm toluene (11 ppm $^{13}C_7H_8$ from natural abundance) which resulted in the accurate 6:1 ratio of peak areas for aromatic resonances ($\delta(^{13}C) \approx 120 - 130$ ppm) to the peak area of the methyl resonance ($\delta(^{13}C) \approx 20$ ppm).

Acknowledgements

We acknowledge The Dow Chemical Company and the National Science Foundation (CBET 1701534) for finanical support for this research, Mr. Linh Bui (University of Minnesota) for invaluable technical discussions, and Mr. Todd Rappe (Minnesota NMR Center) for assistance with NMR experiments. BAJ acknowledges an undergraduate research fellowship administered by the Office of Undergraduate Research at the University of Minnesota.

Appendix A. Supplementary material

Supplementary data associated with this article can be found, in the online version, at https://doi.org/10.1016/j.jcat.2018.10.022.

References

[1] G.A. Olah, A. Goeppert, G.K.S. Prakash, Beyond Oil and Gas: The Methanol Economy, second ed., Wiley-VCH, 2011.
[2] P. Lanzafame, S. Perathoner, G. Centi, Catalyst needs and perspective for integrating biorefineries within the refinery value chain, in: D. Üner (Ed.), Advances in Refining Catalysis, Chemical Industries, CRC Press, 2017.
[3] J.Q. Chen, A. Bozzano, B. Glover, T. Fuglerud, S. Kvisle, Recent advancements in ethylene and propylene production using the UOP/Hydro MTO process, Catal. Today 106 (2005) 103–107.
[4] P. Tian, Y. Wei, M. Ye, Z. Liu, Methanol to olefins (MTO): from fundamentals to commercialization, ACS Catal. 5 (2015) 1922–1938.
[5] B.M. Lok, C.A. Messina, R.L. Patton, R.T. Gajek, T.R. Cannan, E.M. Flanigen, Silicoaluminophosphate molecular sieves: another new class of microporous crystalline inorganic solids, J. Am. Chem. Soc. 106 (1984) 6092–6093.
[6] B.M. Lok, C.A. Messina, R.L. Patton, R.T. Gajek, T.R. Cannan, E.M. Flanigen, Crystalline silicoaluminophosphates, U.S. Patent 4,440,871.
[7] E.M. Flanigen, R.L. Patton, S.T. Wilson, Structural, synthetic and physicochemical concepts in aluminophosphate-based molecular sieves, in: P. Grobet, W. Mortier, E. Vansant, G. Schulz-Ekloff (Eds.), Innovation in Zeolite Materials Science – Proceedings of an International Symposium, Vol. 37 of Stud. Surf. Sci. Catal., Elsevier, 1988, pp. 13–27.
[8] C. Baerlocher, L.B. McCusker, D.H. Olson, Atlas of Zeolite Framework Types, sixth ed., Elsevier, 2007.
[9] J.F. Haw, W. Song, D.M. Marcus, J.B. Nicholas, The mechanism of methanol to hydrocarbon catalysis, Acc. Chem. Res. 36 (2003) 317–326.
[10] W. Song, J.F. Haw, J.B. Nicholas, C.S. Heneghan, Methylbenzenes are the organic reaction centers for methanol-to-olefin catalysis on HSAPO-34, J. Am. Chem. Soc. 122 (2000) 10726–10727.
[11] B. Arstad, S. Kolboe, The reactivity of molecules trapped within the SAPO-34 cavities in the methanol-to-hydrocarbons reaction, J. Am. Chem. Soc. 123 (2001) 8137–8138.
[12] B.P.C. Hereijgers, F. Bleken, M.H. Merete, S. Svelle, K.-P. Lillerud, M. Bjørgen, B. M. Weckhuysen, U. Olsbye, Product shape selectivity dominates the methanol-to-olefins (MTO) reaction over H-SAPO-34 catalysts, J. Catal. 264 (2009) 77–87.
[13] S. Ilias, A. Bhan, Mechanism of the catalytic conversion of methanol to hydrocarbons, ACS Catal. 3 (2013) 18–31.
[14] S. Xu, A. Zheng, Y. Wei, J. Chen, J. Li, Y. Chu, M. Zhang, Q. Wang, Y. Zhou, J. Wang, F. Deng, Z. Liu, Direct observation of cyclic carbenium ions and their role in the catalytic cycle of the methanol-to-olefin reaction over chabazite zeolites, Angew. Chem. Int. Ed. 52 (2013) 11564–11568.
[15] B. Arstad, J.B. Nicholas, J.F. Haw, Theoretical study of the methylbenzene side-chain hydrocarbon pool mechanism in methanol to olefin catalysis, J. Am. Chem. Soc. 126 (2004) 2991–3001.

[16] D. Lesthaeghe, B.D. Sterck, V.V. Speybroeck, G.B. Marin, M. Waroquier, Zeolite shape-selectivity in the *gem*-methylation of aromatic hydrocarbons, Angew. Chem. Int. Ed. 46 (2007) 1311–1314.
[17] C.-M. Wang, Y.-D. Wang, Z.-K. Xie, Z.-P. Liu, Methanol to olefins conversion on HSAPO-34 zeolite from periodic density functional theory calculations: A complete catalytic cycle of side chain hydrocarbon pool mechanism, J. Phys. Chem. C 113 (2009) 4584–4591.
[18] D. Lesthaeghe, V.V. Speybroeck, M. Waroquier, Theoretical evaluation of zeolite confinement effects on the reactivity of bulky intermediates, Phys. Chem. Chem. Phys. 11 (2009) 5222–5226.
[19] C.-M. Wang, Y.-D. Wang, H.-X. Liu, Z.-K. Xie, Z.-P. Liu, Theoretical insight into the minor role of paring mechanism in the methanol-to-olefins conversion within HSAPO-34 catalyst, Micropor. Mesopor. Mater. 158 (2012) 264–271.
[20] V.V. Speybroeck, K. Hemelsoet, K.D. Wispelaere, Q. Qian, J.V. der Mynsbrugge, B.D. Sterck, B.M. Weckhuysen, M. Waroquier, Mechanistic studies on chabazite-type methanol-to-olefin catalysts: insights from time-resolved UV/Vis microspectroscopy combined with theoretical simulations, ChemCatChem 5 (2013) 173–184.
[21] K.D. Wispelaere, K. Hemelsoet, M. Waroquier, V.V. Speybroeck, Complete low-barrier side-chain route for olefin formation during methanol conversion in H-SAPO-34, J. Catal. 305 (2013) 76–80.
[22] C.-M. Wang, Y.-D. Wang, Z.-K. Xie, Verification of the dual cycle mechanism for methanol-to-olefin conversion in HSAPO-34: a methylbenzene-based cycle from DFT calculations, Catal. Sci. Technol. 4 (2014) 2631–2638.
[23] B. Arstad, S. Kolboe, O. Swang, Theoretical study of the heptamethylbenzenium ion. Intramolecular isomerizations and C_2, C_3, C_4 alkene elimination, J. Phys. Chem. A 109 (2005) 8914–8922.
[24] B. Arstad, S. Kolboe, O. Swang, Theoretical study of carbon atom scrambling in benzenium ions with ethyl or isopropyl groups, J. Phys. Org. Chem. 19 (2006) 81–92.
[25] D.M. McCann, D. Lesthaeghe, P.W. Kletnieks, D.R. Guenther, M.J. Hayman, V.V. Speybroeck, M. Waroquier, J.F. Haw, A complete catalytic cycle for supramolecular methanol-to-olefins conversion by linking theory with experiment, Angew. Chem. Int. Ed. 47 (2008) 5179–5182.
[26] D. Lesthaeghe, A. Horré, M. Waroquier, G.B. Marin, V.V. Speybroeck, Theoretical insights on methylbenzene side-chain growth in ZSM-5 zeolites for methanol-to-olefin conversion, Chem. Eur. J. 15 (2009) 10803–10808.
[27] J. Li, Y. Wei, J. Chen, P. Tian, X. Su, S. Xu, Y. Qi, Q. Wang, Y. Zhou, Y. He, Z. Liu, Observation of heptamethylbenzenium cation over SAPO-type molecular sieve DNL-6 under real MTO conversion conditions, J. Am. Chem. Soc. 134 (2012) 836–839.
[28] S. Ilias, A. Bhan, The mechanism of aromatic dealkylation in methanol-to-hydrocarbons conversion on H-ZSM-5: what are the aromatic precursors to light olefins?, J Catal. 311 (2014) 6–16.
[29] M.W. Erichsen, M. Mortén, S. Svelle, O. Sekiguchi, E. Uggerud, U. Olsbye, Conclusive evidence for two unimolecular pathways to zeolite-catalyzed de-alkylation of the heptamethylbenzenium cation, ChemCatChem 7 (2015) 4143–4147.
[30] R.F. Sullivan, C.J. Egan, G.E. Langlois, R.P. Sieg, A new reaction that occurs in the hydrocracking of certain aromatic hydrocarbons, J. Am. Chem. Soc. 83 (1961) 1156–1160.
[31] T. Mole, G. Bett, D. Seddon, Conversion of methanol to hydrocarbons over ZSM-5 zeolite: an examination of the role of aromatic hydrocarbons using ^{13}carbon- and deuterium-labeled feeds, J. Catal. 84 (1983) 435–445.
[32] W. von E. Doering, M. Saunders, H.G. Boyton, H.W. Earhart, E.F. Wadley, W.R. Edwards, G. Laber, The 1,1,2,3,4,5,6-heptamethylbenzenonium ion, Tetrahedron 4 (1958) 178–185.
[33] R.F. Childs, M. Sakai, B.D. Parrington, S. Winstein, Penta- and tetramethylbicyclo[3.1.0]hexenyl cations, J. Am. Chem. Soc. 96 (1974) 6403–6409.
[34] P.W. Gougen, T. Xu, D.H. Barich, T.W. Skloss, W. Song, Z. Wang, J.B. Nicholas, J.F. Haw, Pulse-quench catalytic reactor studies reveal a carbon-pool mechanism in methanol-to-gasoline chemistry on zeolite HZSM-5, J. Am. Chem. Soc. 120 (1998) 2650–2651.
[35] W. Dai, C. Wang, M. Dyballa, G. Wu, N. Guan, L. Li, Z. Xie, M. Hunger, Understanding the early stages of the methanol-to-olefin conversion on H-SAPO-34, ACS Catal. 5 (2015) 317–326.
[36] A. Sassi, M.A. Wildman, H.J. Ahn, P. Prasad, J.B. Nicholas, J.F. Haw, Methylbenzene chemistry on zeolite HBeta: multiple insights into methanol-to-olefin catalysis, J. Phys. Chem. B 106 (2002) 2294–2303.
[37] M. Bjørgen, U. Olsbye, D. Petersen, S. Kolboe, The methanol-to-hydrocarbons reaction: insight into the reaction mechanism from [^{12}C]benzene and [^{13}C]methanol coreactions over zeolite H-beta, J. Catal. 221 (2004) 1–10.
[38] D.W. Breck, Zeolite Molecular Sieves: Structure, Chemistry, and Use, Wiley, 1974.
[39] E.G. Derouane, Zeolites as solid solvents, J. Mol. Catal. A: Chem 134 (1998) 29–45.
[40] R. Gounder, E. Iglesia, The catalytic diversity of zeolites: confinement and solvation effects within voids of molecular dimensions, Chem. Commun. 49 (2013) 3491–3509.
[41] G.L. Price, E. Iglesia, Matrix method for correction of mass spectra in deuterium-exchange applications, Ind. Eng. Chem. Res. 28 (1989) 834–844.
[42] P. Magnoux, P. Roger, C. Canaff, V. Fouche, N.S. Gnep, M. Guisnet, New technique for the characterization of carbonaceous compounds responsible for zeolite deactivation, in: B. Delmon, G. Froment (Eds.), Catalyst Deactivation, Vol. 34 of Stud. Surf. Sci. Catal, Elsevier, 1987, pp. 317–330.
[43] B. Arstad, S. Kolboe, Methanol-to-hydrocarbons reaction over SAPO-34. Molecules confined in the catalyst cavities at short time on stream, Catal. Lett. 71 (2001) 209–212.
[44] S.H. Friedberg, A.J. Insel, L.E. Spence, Linear Algebra, fourth ed., Pearson, 2002.
[45] A. Hwang, D. Prieto-Centurion, A. Bhan, Isotopic tracer studies of methanol-to-olefins conversion over HSAPO-34: the role of the olefins-based catalytic cycle, J. Catal. 337 (2016) 52–56.
[46] M. Boudart, Turnover rates in heterogeneous catalysis, Chem. Rev. 95 (1995) 661–666.
[47] J.F. Hartwig, Organotransition Metal Chemistry: From Bonding to Catalysis, University Science Books, 2010.
[48] A. Hwang, M. Kumar, J.D. Rimer, A. Bhan, Implications of methanol disproportionation on catalyst lifetime for methanol-to-olefins conversion by HSSZ-13, J. Catal. 346 (2017) 154–160.
[49] W. Song, H. Fu, J.F. Haw, Supramolecular origins of product selectivity for methanol-to-olefin catalysis on HSAPO-34, J. Am. Chem. Soc. 123 (2001) 4749–4754.
[50] A. Hwang, A. Bhan, Bifunctional strategy coupling Y_2O_3-catalyzed alkanal decomposition with methanol-to-olefins catalysis for enhanced lifetime, ACS Catal. 7 (2017) 4417–4422.
[51] R. Vomscheid, M. Briend, M.J. Peltre, P. Massiani, P.P. Man, D. Barthomeuf, Reversible modification of the Si environment in template-free SAPO-34 structure upon hydration-dehydration cycles below ca. 400 K, J. Chem. Soc. Chem. Comm. (1993) 544–546.
[52] R. Freeman, H.D.W. Hill, R. Kaptein, Proton-decoupled NMR spectra of Carbon-13 with the nuclear overhauser effect suppressed, J. Magn. Reson. 7 (1972) 327–329.
[53] J.N. Shoolery, Some quantitative applications of ^{13}C NMR spectroscopy, Prog. Nucl. Magn. Reson. Spectrosc. 11 (1977) 79–93.